arXiv:1207.1679v1 [nucl-th] 6 Jul 2012

Electron scattering in isotonic chains as a probe of the proton shell structure of unstable nuclei

X. Roca-Maza[1,2,*] M. Centelles[1], F. Salvat[1], and X. Viñas[1]
[1] *Departament d'Estructura i Constituents de la Matèria and Institut de Ciències del Cosmos,*
Facultat de Física, Universitat de Barcelona, Diagonal 645, 08028 Barcelona, Spain
[2] *INFN, sezione di Milano, via Celoria 16, I-20133 Milano, Italy*

Electron scattering on unstable nuclei is planned in future facilities of the GSI and RIKEN upgrades. Motivated by this fact, we study theoretical predictions for elastic electron scattering in the $N = 82$, $N = 50$, and $N = 14$ isotonic chains from very proton-deficient to very proton-rich isotones. We compute the scattering observables by performing Dirac partial-wave calculations. The charge density of the nucleus is obtained with a covariant nuclear mean-field model that accounts for the low-energy electromagnetic structure of the nucleon. For the discussion of the dependence of scattering observables at low-momentum transfer on the gross properties of the charge density, we fit Helm model distributions to the self-consistent mean-field densities. We find that the changes shown by the electric charge form factor along each isotonic chain are strongly correlated with the underlying proton shell structure of the isotones. We conclude that elastic electron scattering experiments in isotones can provide valuable information about the filling order and occupation of the single-particle levels of protons.

PACS numbers: 21.10.Ft, 25.30.Bf, 13.40.Gp, 21.60.-n

I. INTRODUCTION

Since the 1960's, elastic electron scattering has been utilized to obtain accurate information on the size and shape of nuclei [1–5]. Because electrons and nucleons interact essentially through the electromagnetic force, the nucleus remains rather unperturbed during the scattering process and the analysis of the data is not hampered by uncertainties associated with the strong interaction. Thus, electron scattering is able to provide very clean information about the charge distribution of atomic nuclei [6–8].

Low-energy nuclear physics is nowadays moving very fast towards the domain of exotic nuclei [9]. This is due to the development of successive generations of radioactive-isotope beam (RIB) facilities [10–15], such as FAIR and SPIRAL2 in Europe, FRIB in North America, and HIRFL-CSR, RARF or RIBF in Asia, which will allow studying the properties of nuclei beyond the stability valley. Many interesting effects have already been discovered in exotic nuclei, such as neutron and proton halos, neutron skins, and new magic numbers. These effects may be related to the structure of the nucleon distributions far from stability. As with stable nuclei, one way of exploring the structure of exotic nuclei is through the electromagnetic interaction. For this purpose, a new generation of electron-RIB colliders using storage rings is under construction by RIKEN (Japan) [15, 16] and at GSI (Germany) [17, 18]. It is expected that in the near future the SCRIT project in Japan [19–21] and the ELISe experiment at FAIR in Germany [22] will offer the opportunity of studying the structure of unstable exotic nuclei by means of electron scattering.

On the theoretical side, much work has been devoted to the study of charge distributions of exotic nuclei through calculations of both electron scattering (see e.g. Refs. [23–29]) and proton scattering (see e.g. Ref. [30]). Suda [31] pointed out that in electron scattering off unstable nuclei the maxima and the minima of the charge form factor are very sensitive to the size and the diffuseness of the charge density. This fact has been confirmed by different works that have analyzed the behavior of the charge form factor along isotopic [23, 24, 27, 28] and isotonic [29] chains.

To probe the charge distribution in nuclei, the electron beam energy needs to be of the order of a few hundred MeV. As one deals with relativistic electrons, it is mandatory to solve the elastic scattering problem of Dirac particles in the potential generated by the nuclear charge density. The simplest approach is the plane-wave Born approximation (PWBA) where the initial and final states of the electron are described by Dirac plane waves. The PWBA accounts for many features of electron scattering but it cannot provide an accurate description of the electric charge form factor, in particular near the deeps. The most elaborated calculations of electron-nucleus scattering are obtained by the exact phase-shift analysis of the Dirac equation. This calculation scheme is known as distorted-wave Born approximation (DWBA) [32] and has been used to analyze different aspects of the scattering of electrons by nuclei, see e.g. Refs. [23, 24, 28, 33] and references therein. It is worth noting that for high-energy electron scattering, the eikonal approximation is a reliable choice to deal with the problem [34]; it has been applied in [27, 29, 35] to study electron scattering off proton- and neutron-rich nuclei.

The charge density of the target nucleus is one of the

---

[*] Electronic address: xavier.roca.maza@mi.infn.it

basic ingredients of the electron-nucleus scattering problem. For medium and heavy nuclei, the theoretical charge densities can be calculated in the mean-field approximation using non-relativistic nuclear forces or relativistic mean field (RMF) models. It is known that the overall trends of the elastic scattering of electrons by stable medium and heavy nuclei, are well reproduced by the mean-field charge densities computed with nuclear models that have been calibrated to describe the ground-state properties (in particular the charge radii) of some selected nuclei. However, different nuclear models differ in the fine details and describe with different quality the experimental scattering data. See Ref. [28] for a recent comparison of the elastic electron scattering results predicted by different nuclear mean-field models.

In Ref. [28] we studied elastic electron scattering along the Ca and Sn isotopic chains in DWBA. In that work we reported several correlations among scattering observables and some properties of the nuclear charge density along the isotopic chains [28]. In the present work, we investigate what information on nuclear structure can be gained from the study of elastic electron scattering in the $N = 82$, 50, and 14 isotonic chains, which cover different regions of the mass table. We aim at extracting general trends, according to current mean-field theories, about the behavior of some observables that may be measured in experiments performed with unstable nuclei in the low-momentum transfer region. Our choice of these isotonic chains is motivated by the following reasons. On the one hand, information about the structure of unstable nuclei belonging to the $N = 82$ and $N = 50$ isotonic chains may be relevant in the astrophysical context because some of these nuclei could correspond to waiting points in r-processes [36, 37]. On the other hand, scattering data for light nuclei, such as e.g. those of $N = 14$, are likely to be obtained in future electron scattering facilities such as SCRIT [19–21] and ELISe [22].

The study of elastic electron scattering along isotopic and isotonic chains explores different aspects of the nuclear charge density. The electric charge form factor along an isotopic chain gives information about the effect of the different number of neutrons on the charge density, which becomes more and more dilute and extends to larger distances as the neutron number increases [28]. In an isotonic chain, the changes in the charge form factor primarily inform about the effect of the outer proton single-particle orbitals that are being filled as the atomic number increases in the chain. Thus, our previous [28] and present study together provide a survey of the evolution of the charge form factor with the neutron and proton numbers in different mass regions of the nuclear chart.

The rest of this article is organized as follows. In Section II, we summarize the method employed in our study of electron scattering in isotonic chains. As the basic methodology follows that of Ref. [28], we address the reader to that work and references therein for more details about the relativistic nuclear mean-field theory and about the Dirac partial-wave analysis, which we perform using the ELSEPA code [38] adapted to the nuclear problem. We devote Section III to the presentation and analysis of our numerical results for elastic electron-nucleus scattering in the $N = 82$, 50, and 14 chains. Finally, our conclusions are laid in Section IV.

II. METHOD

To investigate electron scattering in isotonic chains we follow the method developed in Ref. [28]. For completeness, we summarize here the main aspects of this method. The electron beam energy in our investigation is fixed at 500 MeV, which is a typical energy in electron-nucleus scattering experiments. Indeed, rather than discussing directly the differential cross section (DCS), we study the DWBA electric charge form factor because it is almost independent of the electron beam energy in the low-momentum transfer regime, as it can be seen from Fig. 5 of Ref. [28] and from the lower panel of Fig. 4 below. We compute the electric charge form factor as follows:

$$|F(q)|^2 = \left(\frac{d\sigma}{d\Omega}\right)\left(\frac{d\sigma_{\rm Mott}}{d\Omega}\right)^{-1}, \qquad (1)$$

where $d\sigma/d\Omega$ is the DCS calculated in DWBA and $d\sigma_{\rm Mott}/d\Omega$ is the Mott DCS. We use the exact Mott DCS (i.e., the DWBA for a point nucleus) instead of the DCS calculated in PWBA. Therefore, the charge form factor defined by Eq. (1) goes beyond the first Born approximation. It will be denoted by $F_{\rm DWBA}(q)$ hereinafter.

We calculate the charge densities with the relativistic mean-field parametrization G2 [39, 40], which we also employed in Ref. [28]. This nuclear model was constructed as an effective hadronic Lagrangian consistent with the symmetries of quantum chromodynamics. The nucleon density distributions are obtained self-consistently at the mean-field level by numerical solution of the corresponding variational equations. In contrast to most of the nuclear mean-field models that assume point densities, the G2 Lagrangian incorporates the low-energy electromagnetic structure of the nucleon through vector-meson dominance [39, 40]. This implies that the charge density is obtained directly from the self-consistent solution of the mean-field equations without any extra folding with external single-nucleon form factors. It has been shown [39–41] that the G2 relativistic mean-field interaction is a reliable parameter set both for calculations of ground-state properties of nuclei and for predictions of the nuclear equation of state up to supra-normal densities, as well as for predictions of some properties of neutron stars. First calculations of the charge form factor in PWBA with G2 were reported in Ref. [39].

In our calculations, we assume spherical symmetry. The suitability of this assumption for the $N = 82$, 50, and 14 isotones is confirmed, excluding a very few exceptions of small deformation, by mass tables computed either with the non-relativistic Skyrme model [42] or with the relativistic model [43]. Pairing correlations are important for describing open-shell nuclei. We take pairing into account through a modified BCS approach that simulates the continuum (needed for nuclei at the drip lines) through quasi-bound levels which are retained by their centrifugal barrier (neutron levels) or by their centrifugal-plus-Coulomb barrier (proton levels) [44]. The pairing interaction in this approach is described by means of a constant matrix element fitted to reproduce the experimental binding energies of some selected isotopic and isotonic chains as described in Ref. [44]. It is to be mentioned that a mean-field treatment is not expected to be sufficient for light exotic nuclei [25]. Thus, the $N = 14$ isotonic chain studied below (with nuclei from ^{22}O to ^{34}Ca) corresponds to a somewhat limiting case, and the mean-field results should be taken as semiquantitative. The calculations with the G2 model predict a relatively magic character of the neutron numbers $N = 14$ and $N = 16$. These neutron numbers have attracted some attention in recent theoretical and experimental studies as possible new magic numbers in exotic nuclei [45–49].

The use of modeled charge densities and electric charge form factors in the experimental analysis of scattering data has been extensive in the past, and continues to date. This is because in many cases the parameters of the modeled charge densities are directly related with the size of the bulk and surface regions of the nucleus under study. In this way, the parametrized densities help to provide a clear physical interpretation of the electron scattering data. This is the case of the so-called Helm model [50] that we used for some calculations in our previous study of isotopic chains [28]. As one of our aims here is to predict global trends of the electric charge form factor in the low-momentum transfer regime in isotonic chains, we also will perform calculations with Helm model densities fitted to the self-consistent mean-field charge densities. We briefly summarize this procedure in the next subsection.

A. Equivalent Helm charge densities

The original version of the Helm model [50] has been extended in various ways for a more accurate description of the experimental charge densities [51–53]. In the simplest version of the model [50], the charge density is obtained from the convolution of a constant density ρ_0 in a hard sphere of radius R_0 with a Gaussian distribution having variance σ^2. By construction, R_0 gives the effective location of the position of the nuclear surface, and hence characterizes the size of the density profile, whereas the parameter σ is a measure of the thickness of the surface region of the density distribution. The Helm charge density is then given by

$$\rho^{(H)}(\vec{r}) = \int d\vec{r}' f_G(\vec{r} - \vec{r}')\rho_0\Theta(R_0 - r), \tag{2}$$

where

$$f_G(r) = \left(2\pi\sigma^2\right)^{-3/2} e^{-r^2/2\sigma^2}. \tag{3}$$

The two parameters, R_0 and σ^2, of the Helm model determine the charge density as well as the electric charge form factor within the PWBA:

$$F^{(H)}(q) = \int e^{i\vec{q}\cdot\vec{r}}\rho^{(H)}(\vec{r})d\vec{r} = \frac{3}{qR_0} j_1(qR_0)e^{-\sigma^2 q^2/2}, \tag{4}$$

where $j_1(x)$ is the spherical Bessel function. Note that we use natural units throughout the present paper.

We proceed as suggested originally in Ref. [50] to obtain the Helm parameters associated to a given nucleus. First, we require that the first zero of Eq. (4) coincides with the first zero of the mean-field PWBA charge form factor (Fourier transform of the charge density obtained with the G2 model). We will refer to this charge form factor as $F_{\rm PWBA}(q)$ hereinafter. Therefore, the radius of the equivalent Helm density reads

$$R_0 = \frac{x}{q_0}. \tag{5}$$

where $x = 4.49341$ is the first zero of $j_1(x)$ and q_0 is the momentum transfer corresponding to the first zero of $F_{\rm PWBA}(q)$. Second, we determine the variance σ^2 of the Gaussian distribution such that $|F^{(H)}(q_{\rm max})| = |F_{\rm PWBA}(q_{\rm max})|$, where $q_{\rm max}$ is the momentum transfer corresponding to the second maximum of $|F_{\rm PWBA}(q)|$ (the first maximum appears always at $q = 0$ fm). Using Eq. (4), one easily obtains

$$\sigma^2 = \frac{2}{q^2_{\rm max}} \ln\left(\frac{3j_1(q_{\rm max}R_0)}{q_{\rm max}R_0F_{\rm PWBA}(q_{\rm max})}\right). \tag{6}$$

The PWBA form factor obtained in the Helm model neglects the distortion of the electron wave functions due to the electrostatic potential of the nuclear charge distribution. The effect of this Coulomb distortion may be simulated in the Helm model by replacing the momentum transfer q by an effective value [50]. In our study of electron scattering in isotopic chains [28], we found that this correction was important because we were comparing electron-nucleus scattering observables of nuclei with the same proton number, and therefore they exhibited rather small differences. However, this correction can be neglected for the purposes of the present work because it is almost totally masked by the much larger effect from the changing proton number along the isotonic chain.

III. RESULTS: $N = 82$, $N = 50$, AND $N = 14$ ISOTONIC CHAINS

We start with the discussion of the results for the $N = 82$ isotonic chain where the different aspects of our study are described in detail. After that, we extend our study to the $N = 50$ and $N = 14$ isotonic chains.

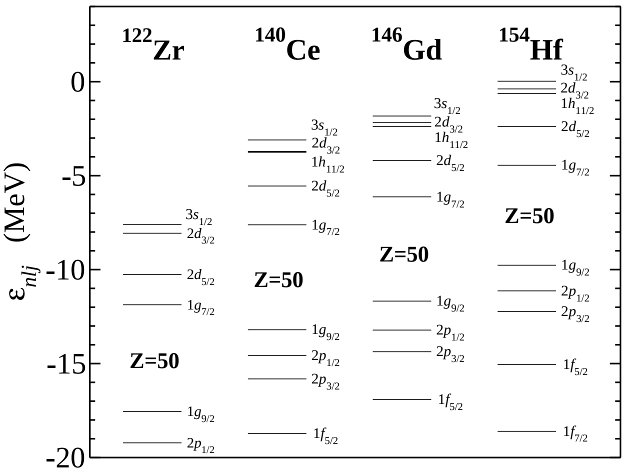

FIG. 1: Energy of the proton single-particle levels for $^{122}_{40}$Zr, $^{140}_{58}$Ce, $^{146}_{64}$Gd and $^{154}_{72}$Hf as computed with the relativistic nuclear mean field interaction G2.

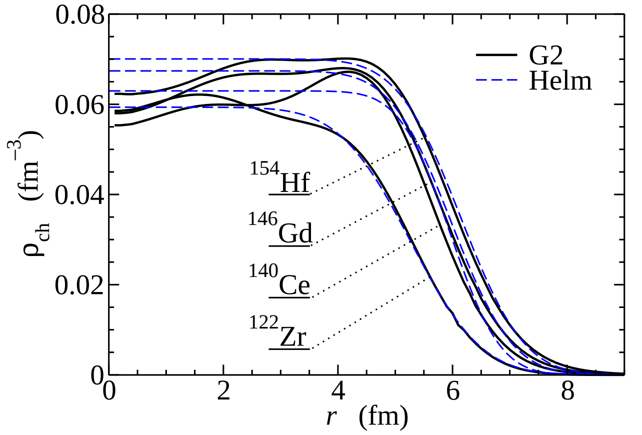

FIG. 2: Charge densities for $^{122}_{40}$Zr, $^{140}_{58}$Ce, $^{146}_{64}$Gd and $^{154}_{72}$Hf as a function of the radial distance to the center of the nucleus according to the covariant model G2 (solid lines) and to the fitted Helm distributions (dashed lines).

A. $N = 82$ isotonic chain

We first analyze the charge densities along the $N = 82$ chain. The ordering and the energy of the different proton single-particle levels, mainly the levels closest to the Fermi level, are quite important for the present study. This is because the corresponding single-particle wave functions determine, to a large extent, the shape of the charge density at the surface region as well as the electric charge form factor in the low-momentum transfer region. Fig. 1 displays the energy of the proton single-particle levels of some selected nuclei of the $N = 82$ isotopic chain. They are representative of proton deficient nuclei ($^{122}_{40}$Zr), stable nuclei ($^{140}_{58}$Ce), proton rich-nuclei ($^{146}_{64}$Gd) and proton drip-line nuclei ($^{154}_{72}$Hf).

The more relevant proton single-particle levels in our analysis of the $N = 82$ isotonic chain are, on the one hand, the $1g_{9/2}$, $1g_{7/2}$ and $2d_{5/2}$ levels (which appear clearly separated in energy) and, on the other hand, the nearly degenerate $1h_{11/2}$, $2d_{3/2}$ and $3s_{1/2}$ levels (which have a very close energy). The $1h_{11/2}$ level shows energy gaps of about 2 and 4 MeV with respect to the $2d_{5/2}$ and $1g_{7/2}$ levels, respectively, and a gap of about 9 MeV with respect to the deeper $1g_{9/2}$ level. This large energy gap is due to the magicity of the proton number $Z = 50$. With increasing mass number these relevant levels are shifted up in energy, roughly as a whole, retaining the same ordering and approximately the same energy gaps. As a consequence of this level scheme, in going from the nucleus $^{122}_{40}$Zr to $^{140}_{58}$Ce the charge densities differ basically by the effects of filling up the $1g_{9/2}$ and $1g_{7/2}$ shells, and in going from $^{140}_{58}$Ce to $^{146}_{64}$Gd the charge densities differ by the occupancy the $2d_{5/2}$ shell. In these proton-rich isotones with mass number above $A = 140$, the pairing correlations play a non-negligible role and therefore the charge densities also get contributions from the $1h_{11/2}$, $2d_{3/2}$, and $3s_{1/2}$ orbitals. Finally, in the case of the drip-line nucleus $^{154}_{72}$Hf, all of the mentioned single-particle wave functions contribute significantly to the charge density. The differences in the charge distribution due to single-particle effects become evident in Fig. 2 where the charge densities of $^{122}_{40}$Zr,$^{140}_{58}$Ce, $^{146}_{64}$Gd, and $^{154}_{72}$Hf computed with the relativistic mean field model G2 are displayed as functions of the radial distance.

The equivalent Helm charge densities of these isotones, with parameters determined as explained in Section II A, are depicted in Fig. 2 by dashed lines. As in the case of isotopes studied in Ref. [28], the quantal oscillations of the mean-field charge densities are nicely averaged by the bulk part of the Helm model densities. In spite of the fact that the surface fall-off of the Helm densities is of Gaussian type, the agreement at the surface between the mean-field and the equivalent Helm charge distributions is in general satisfactory.

The fitted parameters of the equivalent Helm densities along the $N = 82$ isotopic chain, namely R_0 and σ^2, are displayed in the two panels of Fig. 3 as functions of $A^{1/3}$ and A, respectively. The radius R_0 roughly follows a linear trend with $A^{1/3}$ as it can be expected from the increase of the total number of nucleons. The parameter σ^2, which determines the surface thickness of the charge density, shows a non-uniform variation with the mass number A, reflecting the underlying shell structure of the nuclei of this chain.

In our study of isotopic chains [28], we found a similar behavior of the σ^2 parameter but with two important differences. First, the range of variation of σ^2 in isotopic chains is much smaller than the one exhibited by the $N = 82$ isotonic chain. Second, in the case of the Sn isotopes (see Fig. 6 of Ref. [28]) σ^2 displays local minima for ^{132}Sn and ^{176}Sn, pointing out the magicity of the $N = 82$ and $N = 126$ neutron numbers which makes the charge densities of these isotopes more compact. In con-

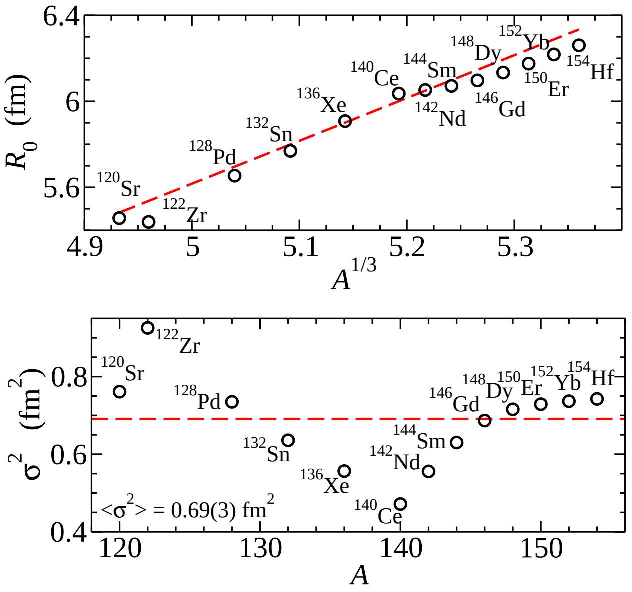

FIG. 3: Upper panel: Mass-number dependence of the Helm parameter R_0 predicted by the covariant mean field model G2 in the $N = 82$ isotonic chain. Lower panel: Mass-number dependence of the Helm parameter σ^2. The average value is depicted by a horizontal dashed line.

trast, in the $N = 82$ isotonic chain, the kinks shown by σ^2 are rather related with the filling of the different proton single-particle orbitals belonging to the major shell between $Z = 50$ and $Z = 82$. In particular, when the $1g_{9/2}$ and $1g_{7/2}$ shells are being filled, i.e., between ${}^{122}_{40}$Zr and ${}^{140}_{58}$Ce, σ^2 decreases almost linearly. The local minimum of σ^2 for ${}^{140}_{58}$Ce points to some magic character of this nucleus. The fact that the σ parameter takes the smaller values in the region around ${}^{140}_{58}$Ce, indicates that the surface of the equivalent charge density is more abrupt at and around this nucleus. When the $2d_{5/2}$ level starts to be appreciably occupied, σ^2 increases again nearly linearly till ${}^{146}_{64}$Gd, where a new kink appears. From ${}^{146}_{64}$Gd to the proton drip line (${}^{154}_{72}$Hf), the value of σ^2 continues to increase, but now with a smaller slope as a consequence of the higher occupancy of the $1h_{11/2}$, $2d_{3/2}$, and $3s_{1/2}$ levels. Therefore, the Helm model parameter σ^2 is extremely sensitive to the evolution of the proton shell structure along an isotonic chain.

We next inspect the main properties of the differential cross sections and electric charge form factors of the $N = 82$ isotones. In the upper panel of Fig. 4 we display for three representative nuclei of the $N = 82$ chain the DCS as a function of the scattering angle θ. The electron beam energy is 500 MeV. The DCS is computed in the DWBA using both the self-consistent mean-field charge densities obtained with the G2 model (solid lines) and the equivalent Helm charge densities (dashed lines). The square modulus of the DWBA electric charge form factor $|F_{\rm DWBA}(q)|^2$ as a function of the momentum transfer $q = 2E\sin(\theta/2)$ is shown in the lower panel of Fig. 4. The empty symbols in the lower panel of this figure correspond to $|F_{\rm DWBA}(q)|^2$ computed at an electron beam energy of 250 MeV. The comparison of the results for $|F_{\rm DWBA}(q)|^2$ at $E = 500$ MeV and $E = 250$ MeV shows that the electric charge form factor defined in Eq. (1) is largely independent of the energy of the beam in the low-momentum transfer domain. Therefore, the analysis of $|F_{\rm DWBA}(q)|^2$ contains the essential trends of the elastic electron-nucleus scattering in this regime.

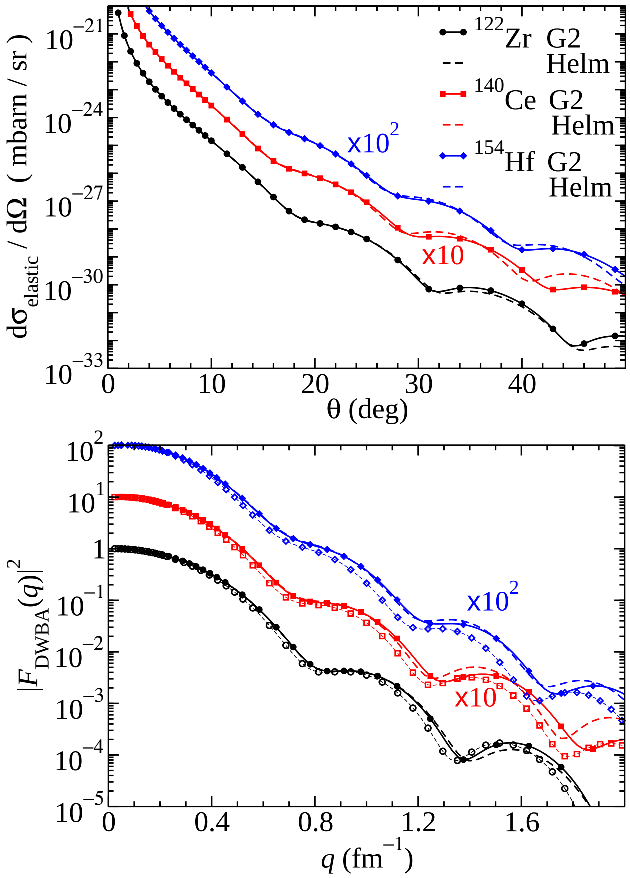

FIG. 4: DCS for elastic electron-nucleus scattering (upper panel) and square charge form factor (lower panel) in ${}^{122}_{40}$Zr, ${}^{140}_{58}$Ce, and ${}^{154}_{72}$Hf at 500 MeV computed in DWBA. The results are shown both for the self-consistent mean-field densities of G2 (solid lines) and for the equivalent Helm distributions fitted to the G2 densities (dashed lines). In the lower panel, we also show by empty symbols the results obtained at 250 MeV using the self-consistent G2 densities.

The dashed lines in the two panels of Fig. 4 correspond to the DWBA result but using the equivalent Helm charge distributions, fitted as explained previously, instead of the self-consistent mean-field densities. One notes an excellent agreement at low-momentum transfers up to 1.5–2 fm^{-1} between the results from the original mean-field densities and from the equivalent Helm charge densities. This fact reassures one of the ability of the parametrized Helm distributions to describe global

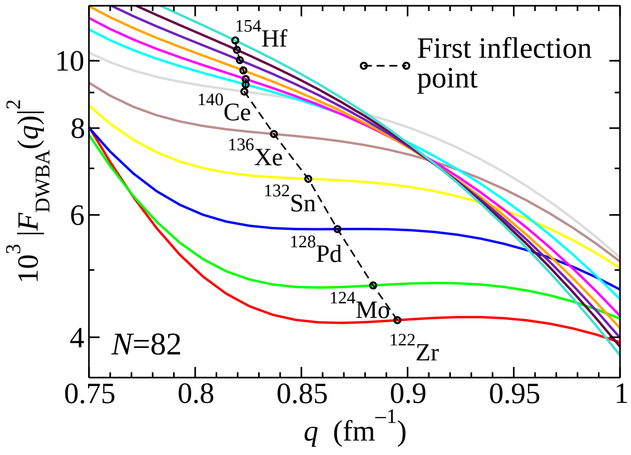

FIG. 5: Evolution of the square modulus of the DWBA electric charge form factor with the momentum transfer q along the $N = 82$ isotonic chain as predicted by G2 at an electron beam energy of 500 MeV. The momentum transfer corresponding to the first inflection point for each isotone is shown by circles.

trends of elastic electron-nucleus scattering at low q, as it was also found in Ref. [28] for isotopes.

In medium and heavy mass nuclei, the first oscillations of the DCS and of the square charge form factor computed within the DWBA usually do not show clean local minima but they rather show inflection points. As we can see in Fig. 4, this is the situation for the first oscillation of the DCS and of $|F_{\rm DWBA}(q)|^2$ in the $N = 82$ isotonic chain. In the absence of an explicit minimum, the first inflection point (IP) is the best candidate to characterize the relevant properties of the electric charge form factor at low q as we discussed in Ref. [28]. In Fig. 5 we plot $|F_{\rm DWBA}(q)|^2$ for the $N = 82$ isotones in a magnified view around the first IP. The value of $|F_{\rm DWBA}(q)|^2$ at the first IP is depicted by circles for each nucleus. In agreement with earlier literature [29], the momentum transfer at the first inflection point ($q_{\rm IP}$) shows an inward shifting and the value of $|F_{\rm DWBA}(q_{\rm IP})|^2$ shows an upward trend with increasing mass number along the isotonic chain.

Let us discuss possible correlations of the DWBA charge form factor at low-momentum transfer with the parameters R_0 and σ of the equivalent Helm charge density, as we did in our previous analysis of isotopic chains [28]. If we first look at the analytical expression of the charge form factor predicted by the Helm model, cf. Eq. (4), it suggests to use qR_0 and $\sigma^2 q^2$ as the natural variables to investigate the variation of this quantity. In the $q \to 0$ limit, Eq. (4) can be written as

$$F^{(H)}(q \to 0) = 1 - \frac{1}{10} q^2 \left(5\sigma^2 + R_0^2\right) + \mathcal{O}[q^4]. \qquad (7)$$

This result points towards a linear correlation with the mean square radius $\langle r_{_H}^2 \rangle$ of the Helm distribution [50] due to the fact that

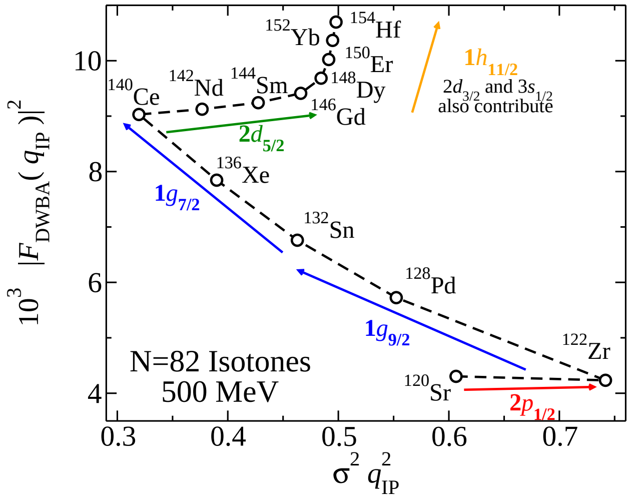

FIG. 6: Square modulus of the electric charge form factor in DWBA at the first inflection point ($q_{\rm IP}$) as a function of $\sigma^2 q_{\rm IP}^2$ predicted by the RMF model G2 for the $N = 82$ isotones.

$$\langle r_{_H}^2 \rangle = \frac{3}{5} \left(5\sigma^2 + R_0^2\right). \qquad (8)$$

However, the correlation suggested by this approximation is not fullfiled by the DWBA calculations in the relevant region of momentum transfers for our study. For this reason, we have further investigated the relation of $|F_{\rm DWBA}(q_{\rm IP})|^2$ with $q_{\rm IP}^2 R_0^2$ and $\sigma^2 q_{\rm IP}^2$ separately. We show in Fig. 6 the behavior of $|F_{\rm DWBA}(q_{\rm IP})|^2$ as a function of the value of $\sigma^2 q_{\rm IP}^2$ since it will be very instructive to understand the influence of the proton shell structure on elastic electron scattering in the isotonic chains.

The non-uniform variations seen in Fig. 6 along the horizontal axis are basically due to the Helm parameter σ^2 rather than to $q_{\rm IP}^2$. This is because of the fact that if we compare the relative change along the isotopic chain found in the quantities σ and $q_{\rm IP}$ (cf. Figs. 3 and 5, respectively), it is much larger in the case of the σ parameter. Hence, the information along the horizontal axis of Fig. 6 is sensitive to the filling order of the single-particle levels contributing to the charge density at the surface region.

The non-uniform variation shown by $|F_{\rm DWBA}(q_{\rm IP})|^2$ along the vertical axis in Fig. 6 can be qualitatively understood in terms of the single-particle contributions to the PWBA electric charge form factor. To this end we plot in Fig. 7 the contribution to the PWBA form factor from the individual proton orbitals:

$$f_{nlj}(q) \equiv \int d\vec{r} \mid \psi_{nlj}(\vec{r}) \mid^2 e^{i\vec{q}\cdot\vec{r}}, \qquad (9)$$

where $\psi_{nlj}(\vec{r})$ is the wave function of a proton level with quantum numbers n, l, and j. Note that (9) does not include the occupation probability factors (v_{nlj}) and de-

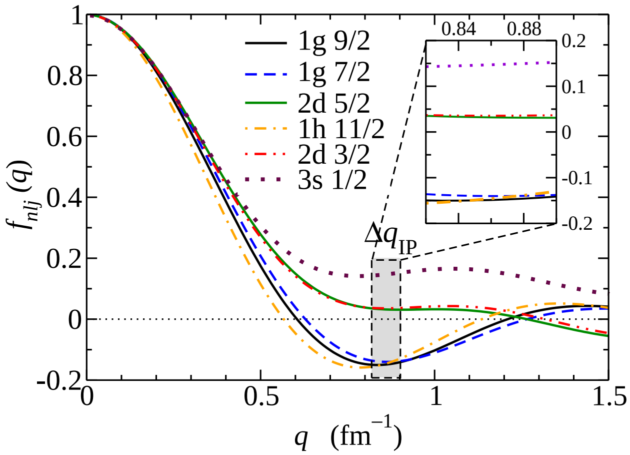

FIG. 7: Shell contribution to the form factor of the last occupied levels in PWBA [see Eq. (9)] as a function of the momentum transfer, calculated in the nucleus $^{154}_{72}$Hf with the G2 mean field model. The shaded region indicates the range of observed q_{IP} values in the calculations of the form factor in DWBA for the $N = 82$ isotonic chain.

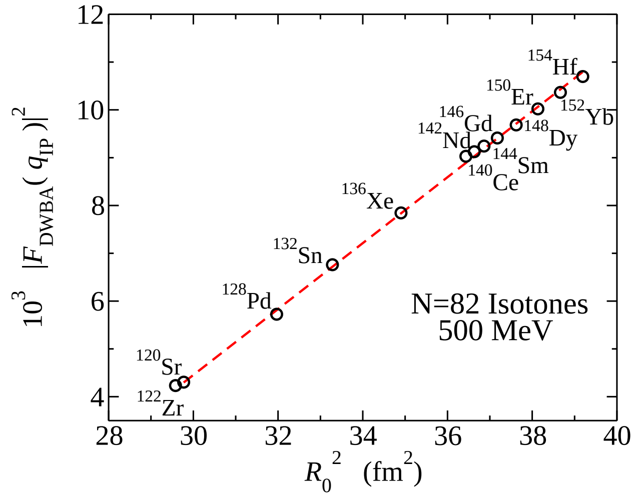

FIG. 8: Square modulus of the electric charge form factor in DWBA at the first inflection point (q_{IP}) as a function of R_0^2 predicted by the RMF model G2 for the $N = 82$ isotones.

generacies $(2j + 1)$, i.e.,

$$F_{\mathrm{PWBA}}(q) = \frac{1}{Z} \sum_{nlj} (2j + 1) v_{nlj} f_{nlj}(q). \qquad (10)$$

In Fig. 7 we depict $f_{nlj}(q)$ for the orbitals close to the Fermi level in the nucleus $^{154}_{72}$Hf, which can be considered as representative of the level scheme of the $N = 82$ isotopic chain. First, one notes that the single-particle contributions $f_{nlj}(q)$ to the PWBA electric charge form factor do not have the same sign in the range of momentum transfers of interest in our analysis. Therefore, strong interference effects may occur among these single-particle contributions. In particular, we can see in Fig. 7 that in the region around q_{IP} the contributions from the $1g_{9/2}$, $1g_{7/2}$, and $1h_{11/2}$ orbitals are negative, while the contributions from the $3s_{1/2}$, $2d_{5/2}$, and $2d_{3/2}$ orbitals are positive. The PWBA form factor corresponding to the underlying $Z = 40$ core is negative. Therefore, when the $1g_{9/2}$ and $1g_{7/2}$ orbitals are occupied—in passing from $^{122}_{40}$Zr to $^{140}_{58}$Ce—the square modulus of the PWBA form factor increases. When on top of this configuration, the $2d_{5/2}$ orbital is filled in $^{146}_{64}$Gd, the square modulus of the PWBA charge form factor decreases due to the positive sign of the contribution of this level around q_{IP}. This simple pattern in the uniform filling picture is slighlty modified due to the pairing correlations that introduce additional mixing with the contributions from the $2d_{3/2}$, $3s_{1/2}$, and $1h_{11/2}$ orbitals. In spite of this, the simple PWBA description is quite useful to help us interpret the changes of $|F_{\mathrm{DWBA}}(q_{\mathrm{IP}})|^2$ from $^{122}_{40}$Zr to $^{146}_{64}$Gd. The subsequent increase shown by $|F_{\mathrm{DWBA}}(q_{\mathrm{IP}})|^2$ from $^{146}_{64}$Gd to $^{154}_{72}$Hf can also be understood in this schematic picture since the PWBA charge form factor of $^{146}_{64}$Gd is globally negative and the additional contribution of the $1h_{11/2}$ orbital also is negative for q values near q_{IP}.

The discussed theoretical results pinpoint the importance of the filling order of the proton single-particle levels in elastic electron scattering off exotic nuclei. Therefore, future experiments such as those planned in the upgrades of the GSI and RIKEN facilities may become excellent probes of the shell structure of exotic nuclei and may also confirm or refute the theoretical predictions of new magic numbers.

Regarding the relation of $|F_{\mathrm{DWBA}}(q_{\mathrm{IP}})|^2$ with $q_{\mathrm{IP}}^2 R_0^2$, we have not found a simple behavior. In spite of this, we have observed that $|F_{\mathrm{DWBA}}(q_{\mathrm{IP}})|^2$ and the square of the Helm radius R_0^2 show a rather similar behavior as a function of the mass number in the isotonic chain. This suggests plotting $|F_{\mathrm{DWBA}}(q_{\mathrm{IP}})|^2$ against R_0^2, which we do in Fig. 8. One observes a good linear correlation between both quantities. This correlation indicates that the parameter of the Helm model which measures the size of the bulk part of the density profile of each isotone governs the magnitude of the electric charge form factor at low momentum transfer.

To conclude this section, we would like to note that some of the details of the predicted single-particle energies, energy gaps, and filling order of the orbitals change to some extent if in our calculations we use other RMF models or Skyrme forces instead of the G2 interaction. In particular, this is due to the fact that we are exploring regions of the nuclear chart beyond the region where the parameters of these effective nuclear interactions have been calibrated. However, the basic conclusion to be emphasized, i.e., the manifest sensitivity of some electron scattering observables to the proton shell structure of the isotones, is a robust feature that comes out regardless of the effective nuclear model.

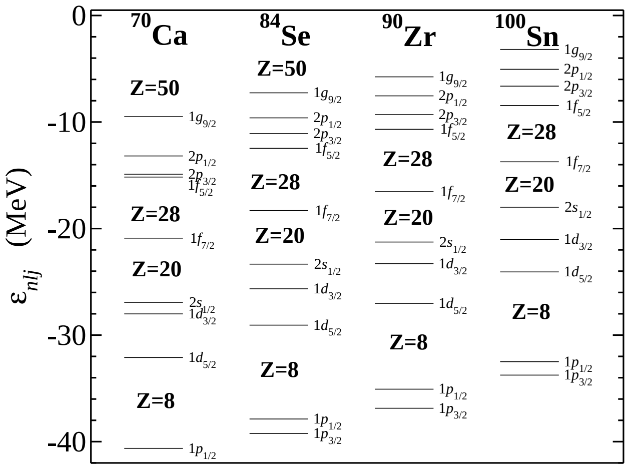

FIG. 9: Energy of the proton single-particle levels for $^{70}_{20}$Ca, $^{84}_{34}$Se, $^{90}_{40}$Zr, and $^{100}_{50}$Sn as computed with the G2 parameter set.

B. $N = 50$ isotonic chain

The more relevant proton single-particle orbitals for our study of the $N = 50$ chain are the $1f_{7/2}$, $1f_{5/2}$, $2p_{3/2}$, $2p_{1/2}$, and $1g_{9/2}$ orbitals. They cover two major shells between Ca and Sn. This set of proton energy levels computed with the G2 parametrization is displayed in Fig. 9 for some selected isotones. We can see that these levels move up in energy, roughly as a whole, when the mass number increases in going from proton-deficient nuclei ($^{70}_{20}$Ca) to stable nuclei ($^{84}_{34}$Se, $^{90}_{40}$Zr) and to proton drip-line nuclei ($^{100}_{50}$Sn).

The parameters R_0 and σ^2 of the Helm model distributions fitted to the mean-field charge densities of the $N = 50$ isotones are displayed in Fig. 10. The global features are similar to the case of the $N = 82$ chain. The R_0 parameter, which represents the effective location of the surface of the nucleus, approximately follows a linear trend with $A^{1/3}$. The mass-number dependence of σ^2 again displays a non-uniform trend, originated by the filling of the different proton single-particle orbitals. We see that σ^2 decreases in filling the $1f_{7/2}$ shell from $^{70}_{20}$Ca to $^{78}_{28}$Ni, it remains roughly constant when the $1f_{5/2}$ level is being filled up to $^{84}_{34}$Se, it increases when the $2p_{3/2}$ and $2p_{1/2}$ shells are occupied till $^{90}_{40}$Zr, and it then decreases until the proton drip-line nucleus $^{100}_{50}$Sn is reached by filling the $1g_{9/2}$ level. Therefore, the more abrupt (smaller σ) equivalent charge densities predicted by the G2 model in the $N = 50$ isotonic chain correspond to nuclei between the doubly-magic, proton-deficient $^{78}_{28}$Ni nucleus and the more stable $^{84}_{34}$Se nucleus, where mainly the $1f_{5/2}$ shell has been filled. In these nuclei, the occupancy of the $2p_{3/2}$, $2p_{1/2}$, and $1g_{9/2}$ levels due to the pairing correlations is rather small.

The square modulus of the DWBA electric charge form factor for an electron beam energy of 500 MeV is displayed against $\sigma^2 q_{\rm IP}^2$ in Fig. 11. As in the case of the $N = 82$ isotones, the behavior of $\sigma^2 q_{\rm IP}^2$ is dominated by the Helm parameter σ. This is because the relative variation of σ^2 (see Fig. 10) is much larger than the relative variation of $q_{\rm IP}^2$ along the isotonic chain. The change of $|F_{\rm DWBA}(q_{\rm IP})|^2$ along the $N = 50$ chain shows, globally, an increasing trend with the mass number. We can appreciate in Fig. 11 that although the variation of $|F_{\rm DWBA}(q_{\rm IP})|^2$ is almost linear when a specific pro-

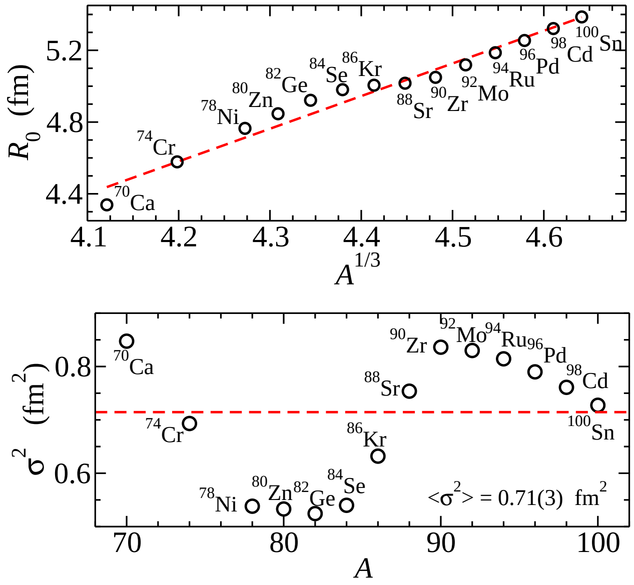

FIG. 10: Upper panel: Mass-number dependence of the Helm parameter R_0 predicted by the covariant mean field model G2 in the $N = 50$ isotonic chain. Lower panel: Mass-number dependence of the Helm parameter σ^2. The average value is depicted by a horizontal dashed line.

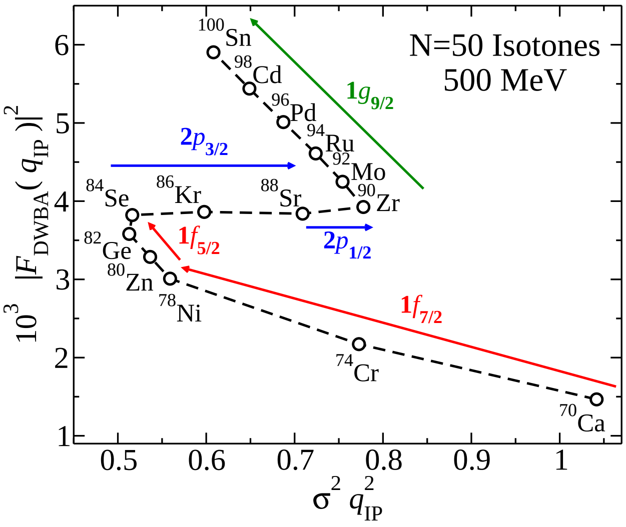

FIG. 11: Square modulus of the electric charge form factor in DWBA at the first inflection point ($q_{\rm IP}$) as a function of $\sigma^2 q_{\rm IP}^2$ predicted by the RMF model G2 for the $N = 50$ isotones.

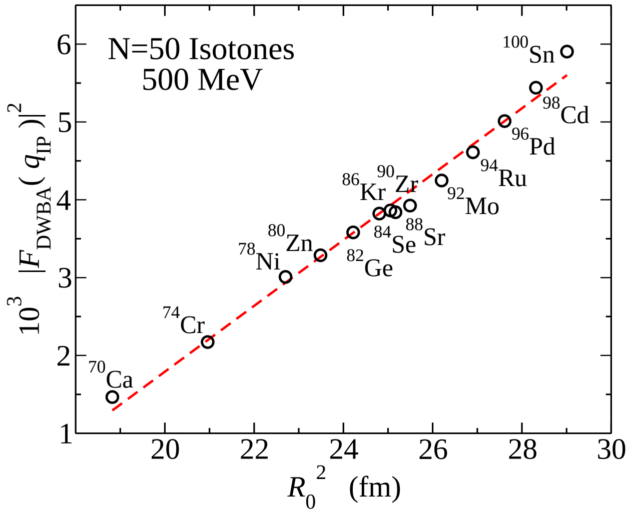

FIG. 12: Square modulus of the electric charge form factor in DWBA at the first inflection point ($q_{\rm IP}$) as a function of R_0^2 predicted by the RMF model G2 for the $N = 50$ isotones.

ton orbital is being occupied, drastic changes of slope take place when a new shell starts to be significantly occupied. Recalling the simplified PWBA picture, cf. Eqs. (9) and (10), we find that in the region of q values around $q_{\rm IP}$ the contribution to the electric charge form factor from the $1f$ and $1g$ orbitals is negative, while the contribution from the $2p$ orbitals is positive. This fact is consistent with the behavior shown by $|F_{\rm DWBA}(q_{\rm IP})|^2$ in Fig. 11. That is, $|F_{\rm DWBA}(q_{\rm IP})|^2$ increases in passing from ${}^{70}_{20}$Ca to ${}^{84}_{34}$Se, basically due to the filling of the $1f_{7/2}$ and $1f_{5/2}$ shells, and then its value is practically quenched up to ${}^{90}_{40}$Zr because the $2p_{3/2}$ and $2p_{1/2}$ orbitals contribute with opposite sign to the $1f$ orbitals. When the $1g_{9/2}$ level is appreciably occupied in approaching the proton drip line, the value of $|F_{\rm DWBA}(q_{\rm IP})|^2$ increases again with a nearly constant rate. Finally, in Fig. 12 we see that $|F_{\rm DWBA}(q_{\rm IP})|^2$ of the $N = 50$ isotones shows a good linear correlation with the square of the Helm parameter R_0.

C. $N = 14$ isotonic chain

In this section we discuss the lightest isotonic chain analyzed in our work. Although the present findings are to be taken with some reservations because the mean-field approach is not best suited for light-mass exotic nuclei, we note that similar general trends to those observed in the heavier-mass isotonic chains also appear in the $N = 14$ chain.

In Fig. 13 we display the neutron (upper panel) and proton (lower panel) single-particle levels computed with the G2 interaction for the $N = 14$ isotonic chain, from the very proton-deficient nucleus ${}^{22}_{8}$O to the very proton-rich nucleus ${}^{34}_{20}$Ca. As expected, the neutron single-particle levels become more bound with increasing mass number. In addition to the prominent energy gap at $N = 8$ seen in the whole chain, it may be noticed that the $1d_{5/2}$ neutron level becomes progressively more isolated when the mass number increases, which points to some magic character of the neutron number $N = 14$ in the calculation with the G2 model. This magic character is confirmed by the vanishing neutron pairing gap found in our calculation from ${}^{26}_{12}$Mg to ${}^{34}_{20}$Ca. It may be observed that the G2 model also predicts a slightly magic character of the neutron number $N = 16$ towards the neutron drip line. Actually, we see in Fig. 13 that the relatively magic trend of $N = 14$ increases from the proton-poor side (${}^{22}_{8}$O) to the proton-rich side (${}^{34}_{20}$Ca) of the chain, while the somewhat magic trend of $N = 16$ decreases from ${}^{22}_{8}$O to ${}^{34}_{20}$Ca.

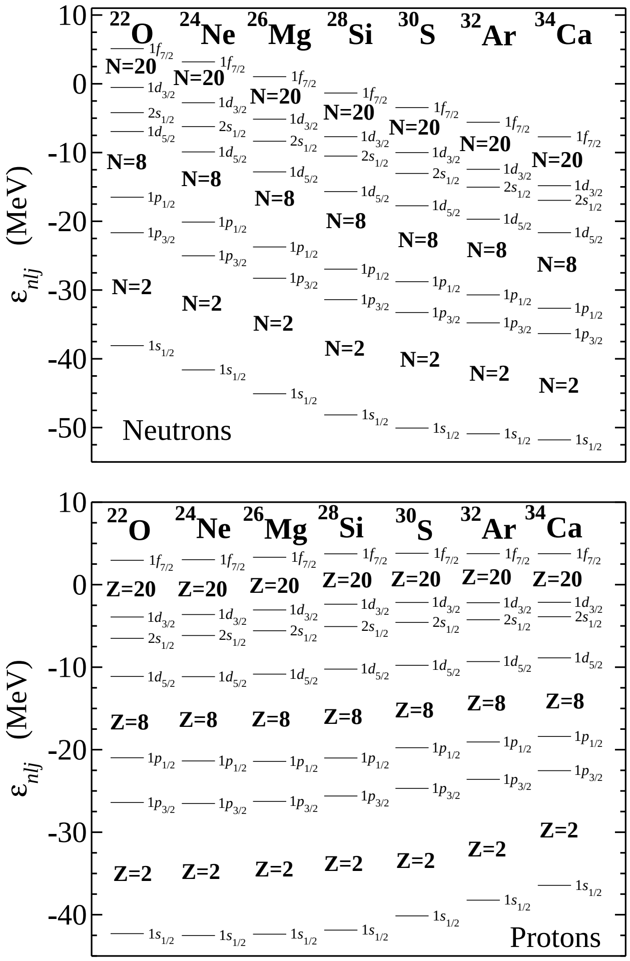

FIG. 13: Energy of the neutron (upper panel) and proton (lower panel) single-particle levels for ${}^{22}_{8}$O, ${}^{24}_{10}$Ne, ${}^{26}_{12}$Mg, ${}^{28}_{14}$Si, ${}^{30}_{16}$S, ${}^{32}_{18}$Ar and ${}^{34}_{20}$Ca as computed with the G2 parameter set.

The more relevant proton single-particle orbitals for our study of the $N = 14$ chain belong to the s-d major shell. The energy levels of this proton major shell (see the lower panel of Fig. 13) lie approximately at the same energy for all the nuclei from ${}^{22}_{8}$O to ${}^{34}_{20}$Ca, with roughly

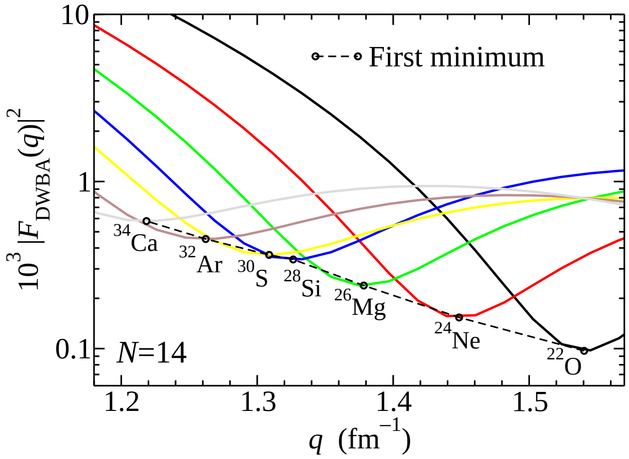

FIG. 14: Evolution of the square modulus of the DWBA electric charge form factor with the momentum transfer q along the $N = 14$ isotonic chain as predicted by G2 at an electron beam energy of 500 MeV. The momentum transfer corresponding to the first minimum for each isotone is shown by circles.

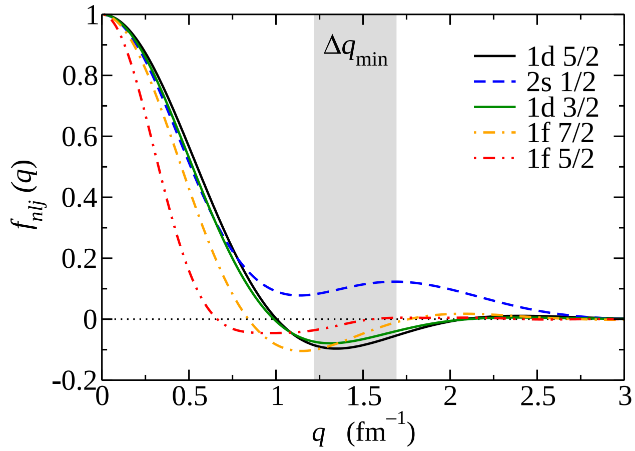

FIG. 15: Shell contribution to the form factor of the last occupied levels in PWBA [see Eq. (9)] as a function of the momentum transfer. The shaded region indicates the range of observed $q_{\rm min}$ values in the calculations of the form factor in DWBA for the $N = 14$ isotonic chain.

constant energy gaps. The $1d_{5/2}$ and $2s_{1/2}$ proton levels exhibit a considerable energy gap between them in this isotonic chain according to the predictions of the G2 model. It is to be mentioned that due to the pairing correlations, the proton levels $1f_{7/2}$ and $1f_{5/2}$ (the latter is not displayed in Fig. 13) also play some role in our calculation of the mean-field charge densities. These levels simulate to a certain extent the effect of the continuum due to their quasi-bound character owing to the Coulomb and centrifugal barriers [54].

In Fig. 14 we display a magnified view of $|F_{\rm DWBA}(q)|^2$ against the momentum transfer for the $N = 14$ isotonic chain. We see that in this chain of lower mass, the inflection point that was found after the first oscillation of the charge form factor in the heavier chains $N = 50$ and $N = 82$ becomes a clearly well defined local minimum. Thus, for the discussion of the $N = 14$ chain we focus on the properties of $|F_{\rm DWBA}(q)|^2$ at its first minimum ($q_{\rm min}$). The value of $|F_{\rm DWBA}(q_{\rm min})|^2$ (shown by the circles in Fig. 14) increases when the value of the momentum transfer at the first minimum decreases, i.e., $|F_{\rm DWBA}(q_{\rm min})|^2$ grows with increasing mass number in the chain. Though the increase of $|F_{\rm DWBA}(q_{\rm min})|^2$ in Fig. 14 is roughly linear with $q_{\rm min}$, one notes a kink at the point corresponding to the $^{28}_{14}$Si nucleus. As we can realize from Fig. 15 in the schematic PWBA picture, this kink is originated by cancellation effects between the opposite contributions to the charge form factor around $q_{\rm min}$ coming from the single-particle wave function of the $1d$ proton level (negative contribution) and of the $2s$ proton level (positive contribution).

The upper panel of Fig. 16 shows that the parameter R_0 of the equivalent Helm charge densities displays, as in the heavier isotonic chains, an overall linear increasing trend with $A^{1/3}$. In turn, the variation of the Helm parameter σ reflects the underlying shell structure of the mean-field charge densities. In the lower panel of Fig. 16, we see that the value of σ^2 remains almost constant between $^{22}_{8}$O and $^{28}_{14}$Si when mainly the $1d_{5/2}$ shell is being filled. From $^{30}_{16}$S on, the $2s_{1/2}$ and $1d_{3/2}$ levels start to be appreciably occupied and σ^2 starts increasing almost linearly with A till the proton-drip line nucleus $^{34}_{20}$Ca.

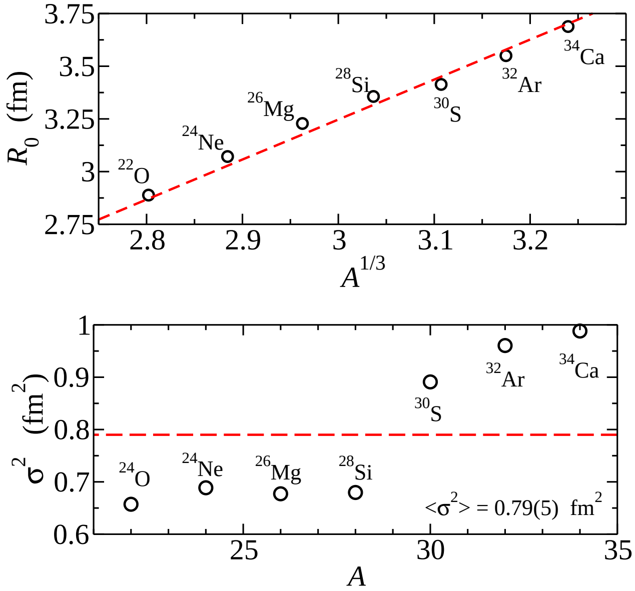

FIG. 16: Upper panel: Mass-number dependence of the Helm parameter R_0 predicted by the covariant mean field model G2 in the $N = 50$ isotonic chain. Lower panel: Mass-number dependence of the Helm parameter σ^2. The average value is depicted by a horizontal dashed line.

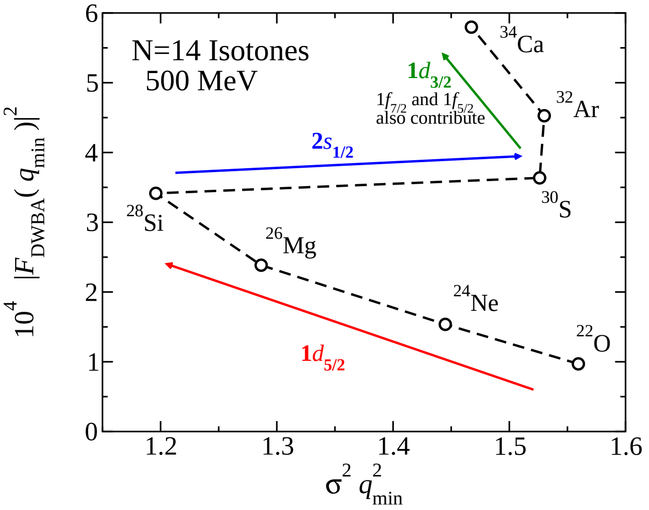

FIG. 17: Square modulus of the electric charge form factor in DWBA at the first minimum ($q_{\rm min}$) as a function of $\sigma^2 q^2_{\rm min}$ predicted by the RMF model G2 for the $N = 14$ isotones.

The influence of the discussed proton shell structure on the electric charge form factor at the first minimum for the $N = 14$ isotones is obvious in Fig. 17, which displays $|F_{\rm DWBA}(q_{\rm min})|^2$ against the value of $\sigma^2 q^2_{\rm min}$. Finally, if we analyze the variation of $|F_{\rm DWBA}(q_{\rm min})|^2$ with the Helm parameter R_0^2, a correlation is found between both quantities (cf. Fig. 18), though now this correlation is less linear than in the heavier isotonic chains $N = 82$ and $N = 50$ (cf. Figs. 8 and 12).

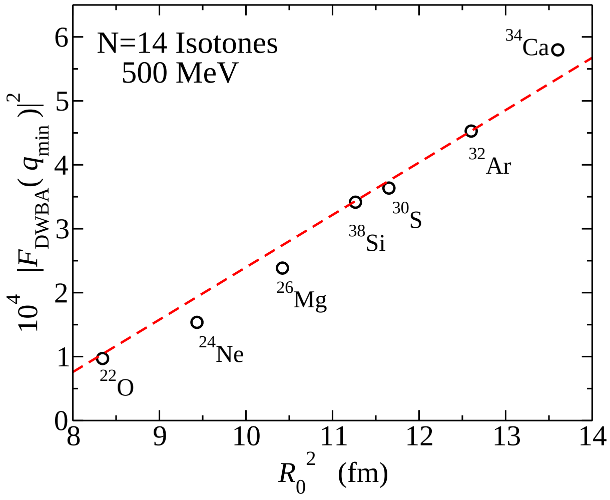

FIG. 18: Square modulus of the electric charge form factor in DWBA at the first minimum ($q_{\rm min}$) as a function of R_0^2 predicted by the RMF model G2 for the $N = 14$ isotones.

IV. SUMMARY AND CONCLUSIONS

In this work we have explored some of the information about nuclear structure that can be obtained from elastic electron scattering in isotones. Due to the fact that the number of protons changes along an isotonic chain, this study primarily probes the effect of the different proton single-particle shells on the elastic electron scattering observables.

We have computed the DWBA differential cross section at an electron beam energy of 500 MeV using the charge densities calculated self-consistently with the covariant nuclear mean-field model G2 [39, 40]. The electric charge form factor has been obtained by taking the ratio of the DWBA differential cross section with the exact (DWBA) Mott differential cross section. The so-defined electric charge form factor is practically independent of the electron beam energy in the low-momentum transfer regime.

We have paid special attention to the electric charge form factor taken at the momentum transfer $q_{\rm IP}$ of the first inflection point, for the $N = 50$ and $N = 82$ chains, or at the momentum transfer $q_{\rm min}$ of the first minimum for the $N = 14$ chain. In agreement with earlier literature, we have found that the values of $q_{\rm IP}$ ($q_{\rm min}$) shift inwards (i.e., they become smaller) and that the values of $|F_{\rm DWBA}(q_{\rm IP})|^2$ ($|F_{\rm DWBA}(q_{\rm min})|^2$) increase when the atomic number increases from the neutron drip line to the proton drip line of the isotonic chain.

The results reveal that along an isotonic chain the DWBA electric charge form factor of each nucleus is extremely sensitive to the underlying proton shell structure. In the simpler PWBA picture, we have found that a particular proton shell may contribute to the electric charge form factor with positive or negative sign in the momentum transfer region of interest in our analysis. The contributions from levels with more than one radial node and small orbital angular momenta have opposite sign to the contributions from levels without radial nodes and large angular momenta. As a consequence, cancellation effects can appear when the different proton shells are successively occupied. Although this description is to some extent masked by pairing correlations, a similar situation is found in the DWBA calculations of the electric charge form factor. Therefore, the rate of change of $|F_{\rm DWBA}(q_{\rm IP})|^2$ or $|F_{\rm DWBA}(q_{\rm min})|^2$ with the proton number along an isotonic chain may vary substantially when a new single-particle orbital enters the nucleus. This suggests that scattering experiments performed on isotones can be effective probes of the proton nuclear shell structure of stable and unstable nuclides.

To investigate the dependence of the first inflection point or first minimum of the electric charge form factor with the basic properties of the charge distribution, we have parametrized the mean-field densities by the Helm model. We have found that the Helm parameter R_0, which measures the mean position of the surface of the charge density, increases with the mass number following roughly an $A^{1/3}$ law. The Helm parameter σ, which is related with the surface thickness of the charge distribution, encodes information from the underlying proton shell structure and, as a consequence, it does not show a definite trend with the mass number. We have also found that at low-momentum tranfers the square modulus of the DWBA electric charge form factor is accurately reproduced if the mean-field densities are replaced by the fitted Helm densities.

In a previous work [28], we noted that correlations between the DWBA electric charge form factor at the first inflection point (or minimum) and the parameters of the Helm densities can provide information about global features of electron scattering along isotopic chains. In the isotonic chains analyzed in the present work, we find that $|F_{\rm DWBA}(q_{\rm IP})|^2$ ($|F_{\rm DWBA}(q_{\rm min})|^2$) shows a rather good linear correlation with the Helm parameter R_0^2, specially in the heavier isotonic chains, while there is no regular behavior with the Helm parameter σ^2 because of its dependence on the last occupied proton orbitals. It should be pointed out that shell effects encoded in the DWBA electric charge form factor are magnified if $|F_{\rm DWBA}(q_{\rm IP})|^2$ ($|F_{\rm DWBA}(q_{\rm min})|^2$) is plotted against $\sigma^2 q_{\rm IP}^2$ ($\sigma^2 q_{\rm min}^2$) along an isotonic chain, providing interesting insights into the proton shell structure of the nuclei of the chain.

In summary, we can conclude that electron scattering on unstable nuclei that is intended to be performed in next-generation facilities [15–22], may become a very useful tool to obtain relevant information about the single-particle shell structure of exotic nuclei.

Acknowledgments

M.C. and X.V. acknowledge the support of the Consolider Ingenio 2010 Programme CPAN CSD2007-00042, Grant No. FIS2011-24154 from MICINN and FEDER, and Grant No. 2009SGR-1289 from Generalitat de Catalunya. F.S. acknowledges support from the Spanish Ministerio de Ciencia e Innovación and FEDER (project No. FPA2009-14091-C02-01) and from the Generalitat de Catalunya (grant SGR 2009-276). X.R. acknowledges support of the Italian Research Project "Many-body theory of nuclear systems and implications on the physics of neutron stars" (PRIN 2008).

---

[1] R. Hofstadter, Rev. Mod. Phys. **28**, 214 (1956).
[2] T. W. Donnelly and J. D. Walecka, Annu. Rev. Nuc. Part. Sci. **25**, 329 (1975).
[3] T. W. Donnelly and I. Sick, Rev. Mod. Phys. **56**, 461 (1984).
[4] E. Moya de Guerra, Phys. Rep. **138**, 293 (1986).
[5] I. Sick, Prog. Part. Nucl. Phys. **47**, 245 (2001).
[6] H. de Vries, C. W. de Jager, and C. de Vries, At. Data Nucl. Data Tables, **36**, 495 (1987).
[7] G. Fricke, C. Bernhardt, K. Heiling, L. A. Schaller, L. Shellenberg, E. B. Shera, and C. W. de Jager, At. Data Nucl. Data Tables **60**, 177 (1995).
[8] I. Angeli, At. Data Nucl. Data Tables **87**, 185 (2004).
[9] *Topical Issue on the Fifth International Conference on Exotic Nuclei and Atomic Masses "ENAM 08"*, edited by J. Äystö, W. Nazarewicz, M. Pfützner, and C. Signorini, Eur. Phys. J. **A 42**, No. 3 (2009).
[10] I. Tanhihata, Prog. Part. Nucl. Phys. **35**, 505 (1995).
[11] H. Geissel, G. Müzenberg, and R. Riisager, Annu. Rev. Nucl. Part. Sci. **45**, 163 (1995).
[12] A. Mueller, Prog. Part. Nucl. Phys. **46**, 359 (2001).
[13] J. W. Xia *et al.*, Nucl. Inst. and Meth. in Phys. Res. **A 488** 11 (2002).
[14] J. W. Xia *et al.*, Construction and Commisioning of HIRFL-CSR, "APAC2007", Indore, India, January 2007.
[15] T. Suda, J. Phys.: Conf. Ser. **267** 012008 (2011).
[16] K. Katayama, T. Suda, and I. Tanihata, Phys. Scr. **T104**, 129 (2003).
[17] An International Accelerator Facility for Beams of Ions and Antiprotons, GSI report 2006. http://www.gsi.de/GSI-Future/cdr/
[18] H. Simon in *Proceedings of the International Workshop XXXII on Gross Properties of Nuclei and Nuclear Excitations*, edited by M. Buballa, J. Knoll, W. Nörenberg, B.-J. Schaefer, and J. Wambach, GSI, Darmstad, (2004), p.290.
[19] T. Suda and M. Wakasugi, Prog. Nucl. Phys. **55**, 417 (2005).
[20] M. Wakasugi, T. Emoto, Y. Furukawa, K. Ishii, S. Ito, T. Koseki, K. Kurita, A. Kuwajima, T. Masuda, A. Morikawa, M. Nakamura, A. Noda, T. Ohnishi, T. Shirai, T. Suda, H. Takeda, T. Tamae, H. Tongu, S. Wang, and Y. Yano, Phys. Rev. Lett. **100**, 164801 (2008).
[21] T. Suda, M. Wakasugi, T. Emoto, K. Ishii, S. Ito, K. Kurita, A. Kuwajima, A. Noda, T. Shirai, T. Tamae, H. Tongu, S. Wang, and Y. Yano, Phys. Rev. Lett. **102**, 102501 (2009).
[22] H. Simon, Nucl. Phys. **A787**, 102 (2007).
[23] A. N. Antonov, D. N. Kadrev, M. K. Gaidarov, E. Moya de Guerra, P. Sarriguren, J. M. Udias, V. K. Lukyanov, E. V. Zemlyanaya, and G. Z. Krumova, Phys. Rev. **C72**, 044307 (2005).
[24] P. Sarriguren, M. K. Gaidarov, E. Moya de Guerra, and A. N. Antonov, Phys. Rev. **C76**, 044322 (2007).
[25] S. Karataglidis and K. Amos, Phys. Lett. **B650**, 148 (2007).
[26] C. A. Bertulani, J. Phys. **G34**, 315 (2007).
[27] Z. Wang and Z. Ren, Phys. Rev. **C70**, 034303 (2004); Phys. Rev. **C71**, 054323 (2005).
[28] X. Roca-Maza, M. Centelles, F. Salvat, and X. Viñas, Phys. Rev. **C78**, 044332 (2008).
[29] Z. Wang Z. Ren, and Y. Fan, Phys. Rev. **C73**, 014610 (2006).
[30] K. Amos, S. Karataglidis and J. Dobaczewski, Phys. Rev. **C70**, 024607 (2004).
[31] T. Suda in *Proceedings of the International Workshop XXXII on Gross Properties of Nuclei and Nuclear Excitations*, edited by M. Buballa, J. Knoll, W. Nörenberg,

B.-J. Schaefer, and J. Wambach, GSI, Darmstad, (2004), p.235.

[32] D. R. Yennie, D. G. Ravenhall, and R. N. Wilson, Phys. Rev. **95**, 500 (1954).

[33] Y. Chu, Z. Ren, Z. Wang, and T. Dong, Phys. Rev. **C82**, 02430 (2010).

[34] A. Baker, Phys. Rev. **134**, B240 (1964).

[35] Y. Chu, Z. Ren, T. Dong, and Z. Wang, Phys. Rev. **C79**, 044313 (2009).

[36] M. Arnould, S. Goriely, and K. Takahashi, Phys. Rep. **450**, 97 (2007).

[37] N. Paar, D. Vretenar, E. Khan, and G. Colò, Rep. Prog. Phys. **70**, 691 (2007).

[38] F. Salvat, A. Jabalonski, and C.J. Powell, Comput. Phys. Commun. **165**, 157 (2005).

[39] R. J. Furnstahl, B. D. Serot, and H.-B. Tang, Nucl. Phys. **A615**, 441 (1997); Nucl. Phys. **A640**, 505 (1998) (E).

[40] B. D. Serot and J. D. Walecka, Int. J. Mod. Phys. **E6**, 515 (1997).

[41] P. Arumugam, B. K. Sharma, P. K. Sahu, S. K. Patra, Tapas Sil, M. Centelles, and X. Viñas, Phys. Lett. **B601** 51, (2004).

[42] J. Dobaczewski, M. V. Stoitsov, and W. Nazarewicz, AIP Conf. Proc. **726**, 51 (2004).

[43] G. A. Lalazissis, S. Raman, and P. Ring, At. Data Nucl. Data Tables **71**, 1 (1999).

[44] M. Del Estal, M. Centelles, X. Viñas and S. K. Patra, Phys. Rev. **C63**, 044321 (2001).

[45] A. Ozawa, T. Kobayashi, T. Suzuki, K. Yoshida, and I. Tanihata, Phys. Rev. Lett. **84**, 5493 (2000).

[46] T. Otsuka, R. Fujimoto, Y. Utsuno, B. A. Brown, M. Honma, and T. Mizusaki, Phys. Rev. Lett. **87**, 082502 (2001).

[47] R. K. Gupta, M Balasubramaniam, S. Kumar, S. K. Patra, G. Münzenberg, and W. Greiner, J. Phys. G: Nucl. Part. Phys. **32**, 565 (2006).

[48] K. Tanaka et al., Phys. Rev. Lett. **104**, 062701 (2010).

[49] N. Wang, M. Liu, and X. Wu, Phys. Rev. **C81**, 044322 (2010).

[50] R. H. Helm, Phys. Rev. **104**, 1466 (1956).

[51] J. Friedrich and N. Voegler, Nucl. Phys. **A373**, 192 (1982).

[52] J. Friedrich, N. Voegler, and P.-G. Reinhard, Nucl. Phys. **A459**, 10 (1986).

[53] D. C. Zheng, N. Yamanishi, and D. W. L. Sprung, Nucl. Phys. **A550**, 89 (1992).

[54] M. Del Estal, M. Centelles, X. Viñas, and S. K. Patra, Phys. Rev. **C63**, 024314 (2001)